J. Fluid Mech. (1977), *vol.* 83, *part* 1, *pp.* 163–176
Printed in Great Britain

A two-dimensional boundary layer encountering a three-dimensional hump

By F. T. SMITH,
Department of Mathematics, Imperial College, London
R. I. SYKES
Meteorological Office, Bracknell, Berkshire, England
AND P. W. M. BRIGHTON
Department of Applied Mathematics and Theoretical Physics, University of Cambridge

(Received 13 January 1977)

A shallow three-dimensional hump disturbs the two-dimensional incompressible boundary layer developed on an otherwise flat surface. The steady laminar flow is studied by means of a three-dimensional extension of triple-deck theory, so that there is the prospect of separation in the nonlinear motion. As a first step, however, a linearized analysis valid for certain shallow obstacles gives some insight into the flow properties. The most striking features then are the reversal of the secondary vortex motions and the emergence of a 'corridor' in the wake of the hump. The corridor stays of constant width downstream and within it the boundary-layer displacement and skin-friction perturbation are much greater than outside. Extending outside the corridor, there is a zone where the surface fluid is accelerated, in contrast with the deceleration near the centre of the corridor. The downstream decay (e.g. of displacement) here is much slower than in two-dimensional flows.

1. Introduction

The basic problem of determining the fluid flow over a hump embedded in a boundary layer has applications in atmospheric dynamics, aerodynamics and other fields (e.g. to the phenomenon of trip-wire transition). Most recently interest in such flows has revived because of the increased concern with air flow over mountains. Both in atmospheric dynamics and in aerodynamics, some considerable study is necessary because of the three-dimensionality in practice and the likelihood of sizeable separations occurring over rough surfaces such as hills, mountain ranges or aircraft wings. These separations can have a drastic effect on the flow drag, and at the same time two-dimensional flow studies (e.g. Smith 1973) may oversimplify the problem.

Here we consider the laminar motion produced when a two-dimensional boundary layer is disturbed by a three-dimensional hump situated on the boundary (figure 1). Since separation is one of the prime concerns in practice, we choose a hump whose size enables us to apply immediately a generalization to fully three-dimensional situations (cf. Smith 1976*a*) of triple-deck theory (Stewartson 1974). This is set out in § 2 below. It is believed that the generalized triple deck will allow solutions regular at separation,

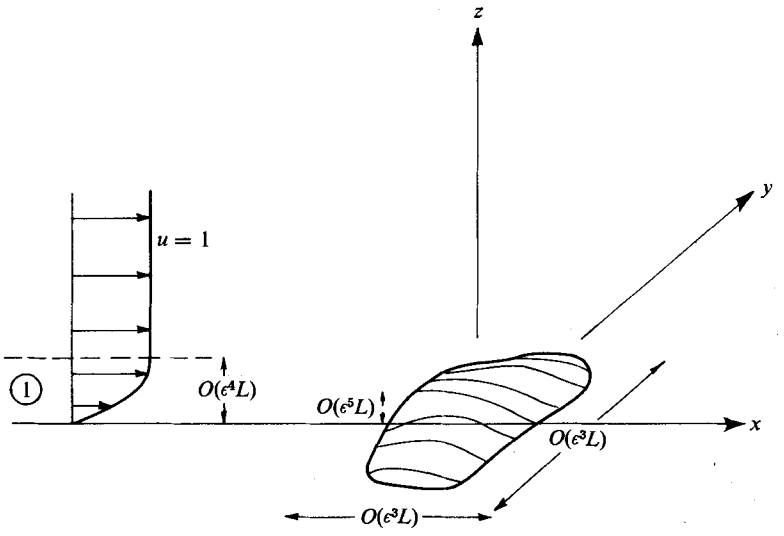

FIGURE 1. The co-ordinate system and the flow problem of an oncoming two-dimensional boundary layer ① encountering a three-dimensional obstacle (shown shaded).

so that our choice of dimensions for the obstacle yields a problem in which three-dimensional separation, displacement and upstream influence (see Sykes 1978) can be incorporated. The 'triple-deck hump' is the shallowest one which can produce separation. If the obstacle is shallower than our choice, the motion is entirely linear and attached flow results. Conversely, if the obstacle is steeper, then there is the likelihood of a gross three-dimensional separation, although if the streamwise length scale is shorter as well the separation may not be gross but then the displacement effect and the upstream influence are diminished (see Brighton (1977), who studies a number of other length scales). Given the importance of the triple-deck size, then, we deal with linearized theory as the first step and examine whether any notable effects are then incurred by the insertion of the three-dimensional obstacle. We find below (see § 4) that indeed there are some pronounced effects. These include the reversal of the vortex motions beyond the peak of the obstacle and a 'corridor' phenomenon in the boundary-layer displacement and axial shear stress. The corridor is a concentrated region that is found to develop behind the obstacle, in which the whole boundary layer is displaced vertically by a relatively large amount. Near the corridor centre the surface fluid is significantly retarded, but away from the centre it is significantly accelerated. Moreover, the corridor does not spread out downstream; rather, it stays of a width comparable with that of the hump. Outside, in a wedge-like zone up to an angle of about 30° from the corridor, there is acceleration of the surface fluid but at a rate generally much less than that within the corridor.

The fluid is assumed to be incompressible and its motion to be laminar and steady. The Cartesian co-ordinates $L(x, y, z)$ denote distances in the directions of the oncoming boundary layer (horizontal), of the surface normal to that boundary layer (horizontal) and of the normal to the surface (vertical) respectively. Here L is the typical length scale of the oncoming boundary layer, and the origin is centred at the obstacle. The fluid velocity is written as $U_\infty(u, v, w)$ and its pressure is $p\rho_\infty U_\infty^2$, where U_∞ and ρ_∞ are

the velocity and density at the edge of the planar boundary layer. The Reynolds number is then $Re = U_\infty L/\nu$, ν being the kinematic viscosity of the fluid, and we suppose that Re is large.

2. The flow structure

The flow problem is summarized in figure 1. It is supposed that the motion far away from the obstacle consists of a two-dimensional boundary layer (wherein $z \sim Re^{-\frac{1}{8}}$) moving in the x direction, outside which the flow is essentially uniform ($u = 1$). If the boundary-layer profile is $U_0(\tilde{z}, x)$, where $\tilde{z} = Re^{\frac{1}{8}} z$, then, near the hump at $x = 0$, $U_0(\tilde{z}, x) \to U_B(\tilde{z})$, say. Here $U_B(\tilde{z})$ has the properties $U_B((\tilde{z}) \sim \lambda\tilde{z}$ as $\tilde{z} \to 0$ and $U_B(\infty) = 1$ and λ is a given positive constant. The flow approaching the hump from upstream is therefore

$$\left.\begin{aligned} u &= U_B(\tilde{z}) + O(x) + O(Re^{-\frac{1}{8}}), \quad v = 0, \\ w &= O(Re^{-\frac{1}{8}}), \quad p = O(Re^{-\frac{1}{8}}) \end{aligned}\right\} \tag{2.1}$$

for x small and $y, \tilde{z} = O(1)$. For convenience we introduce the small parameter ϵ defined by $\epsilon^8 Re = 1$, and mainly consider fully three-dimensional motions below; quasi-two-dimensional cases are mentioned at the end of this section. The three-dimensional hump is assumed to have height $O(L\epsilon^5)$ and horizontal dimensions $O(L\epsilon^3)$. The structure of the flow about the hump then takes on an extended triple-deck form, generalized from that of Smith (1976*a*). Some of its features are familiar from previous triple-deck studies (see Stewartson 1974) but the three-dimensionality plays an active role and so we briefly sketch the development of the solution.

The typical horizontal length scale is $O(L\epsilon^3)$, and in the main deck (I), where $\tilde{z}$ is finite,

$$u = U_B(\tilde{z}) + \epsilon A(X, Y)\, U_B'(\tilde{z}), \quad v = \epsilon^2 D(X, Y)/U_B(\tilde{z}), \tag{2.2a,b}$$

$$w = -\epsilon^2 \frac{\partial A}{\partial X} U_B(\tilde{z}), \quad p = \epsilon^2 P(X, Y), \quad \text{where} \quad \frac{\partial D}{\partial X} = -\frac{\partial P}{\partial Y}. \tag{2.2c–e}$$

Here $(x, y) = \epsilon^3(X, Y)$ and A, D and P are unknown functions of (X, Y) which tend to zero as $X \to -\infty$ [to join with (2.1)] but are assumed to be not identically zero. Solutions (2.2) satisfy the Navier–Stokes equations to leading order. They represent a non-uniform vertical displacement w of the boundary layer accompanied by a small inflow or outflow v generated by the induced horizontal pressure gradient $\partial P/\partial Y$. The vertical displacement then sets up a potential flow in the upper deck (II) just outside I, where X, Y and $\bar{z} = \epsilon^{-3} z$ are $O(1)$. The disturbances to the mainstream $u = 1$ (and $v = w = p = 0$) are $O(\epsilon^2)$ in II and the pressure is governed by Laplace's equation. Matching the pressure and velocities between I and II, and ensuring that the $O(\epsilon^2)$ disturbances decay at the outer edges of II, gives

$$P(X, Y) = -\frac{1}{2\pi} \int_{-\infty}^{\infty} \int_{-\infty}^{\infty} \frac{(\partial^2 A/\partial\xi^2)\, d\xi\, d\eta}{[(X-\xi)^2 + (Y-\eta)^2]^{\frac{1}{2}}}. \tag{2.3}$$

Thus as usual the upper deck serves to provide a relation between the main-deck displacement and the pressure throughout the boundary layer. Lastly, in the lower deck (III), the motion takes on a viscous character. Here

$$(u, v, w, p, z) = (\epsilon U, \epsilon V, \epsilon^3 W, \epsilon^2 P, \epsilon^5 Z) \tag{2.4}$$

and the equations of motion become

$$\frac{\partial U}{\partial X}+\frac{\partial V}{\partial Y}+\frac{\partial W}{\partial Z}=0, \tag{2.5a}$$

$$U\frac{\partial U}{\partial X}+V\frac{\partial U}{\partial Y}+W\frac{\partial U}{\partial Z}=-\frac{\partial P}{\partial X}+\frac{\partial^2 U}{\partial Z^2}, \tag{2.5b}$$

$$U\frac{\partial V}{\partial X}+V\frac{\partial V}{\partial Y}+W\frac{\partial V}{\partial Z}=-\frac{\partial P}{\partial Y}+\frac{\partial^2 V}{\partial Z^2}. \tag{2.5c}$$

The boundary conditions for (2.5) are

$$U=V=W=0 \quad \text{at} \quad Z=hF(X,Y), \tag{2.6a}$$

$$U\sim\lambda(Z+A(X,Y)), \quad V\sim D(X,Y)/\lambda Z \quad \text{as} \quad Z\to\infty, \tag{2.6b}$$

$$U\to\lambda Z, \quad V\to 0, \quad W\to 0, \quad P\to 0 \quad \text{as} \quad X\to-\infty, \tag{2.6c}$$

together with the pressure–displacement relation (2.3) and (2.2*e*). Conditions (2.6) reflect (*a*) the no-slip constraint at the hump ($z=h\epsilon^5F(X,Y)$, h being an $O(1)$ constant), (*b*) the matching with the main deck and (*c*) the continuation with the oncoming profile of (2.1).

Perhaps the most striking feature of the viscous flow is the large size of v in (2.4), implied by the growth of (2.2*b*) at the lower edge of the main deck and required also by mass conservation. It means that the secondary flow (v,w) in III is basically one-dimensional ($v\gg w$), in contrast with that in I, where $v\sim w$. Again, the velocity profile in the Y direction must be jetlike, being zero both at the hump and in the outer reaches of III. For a three-dimensional hump, the non-uniform vertical displacement of the majority of the boundary layer causes a non-uniform pressure variation, through the potential flow outside, and so a non-uniform pressure is transmitted back through the boundary layer. In I, this induced pressure force has only a minor effect on the streamwise and vertical flow. But simply through conservation of momentum, it gives rise directly to the horizontal motion normal to the oncoming stream in I. The velocity of the latter motion must then increase near the wall, to compensate for the reduction in the oncoming velocity, and in III it interacts significantly with the streamwise velocity itself, being of the same order of magnitude.

The whole flow about the hump depends on the solution to the viscous problem (2.5), with conditions (2.6), (2.3) and (2.2*e*). The main-deck and upper-deck flows respond passively to the behaviour in the lower deck. A numerical approach is intended for the basic problem when h is $O(1)$ (Sykes 1978). Flow separation then would seem a likelihood and would possibly be a regular phenomenon, as in the two-dimensional studies of nonlinear triple-deck problems (Stewartson & Williams 1969; Smith & Stewartson 1973). As a first step, however, we discuss in §§ 3 and 4 the linearized solutions relevant when h is small.

It seems worth while noting here that, if the hump has length $\gg L\epsilon^3$ in the y direction, then the motion is quasi-two-dimensional. For example, for a hump whose horizontal dimension normal to the mainstream is $O(L)$, v is $O(\epsilon^5)$ in I, $O(\epsilon^5)$ in II and $O(\epsilon^4)$ in III. The equations controlling U, W and P are then two-dimensional ones, and v follows from a linear equation. The results in § 4 confirm this.

3. Linearized theory ($h \ll 1$)

If h is small the oncoming profile is only slightly perturbed by the hump, and the solution is described by

$$U = \lambda Z + h\bar{U}, \quad (V, W, P, A, D) = h(\bar{V}, \bar{W}, \bar{P}, \bar{A}, \bar{D}). \tag{3.1}$$

Terms of order h^2 are neglected here and in (2.5), which gives linear equations for the barred variables in (3.1). To solve (3.1) use is made of the double Fourier transform, denoted by ** and defined by

$$\bar{U}^{**}(k, l, Z) = \int_{-\infty}^{\infty} \int_{-\infty}^{\infty} e^{-ikX - ilY} \bar{U}(X, Y, Z)\, dX\, dY. \tag{3.2}$$

Then we have the controlling equations

$$ik\bar{U}^{**} + il\bar{V}^{**} + \partial \bar{W}^{**}/\partial Z = 0, \tag{3.3a}$$

$$\lambda ikZ\bar{U}^{**} + \lambda \bar{W}^{**} = -ik\bar{P}^{**}(k, l) + \partial^2 \bar{U}^{**}/\partial Z^2, \tag{3.3b}$$

$$\lambda ikZ\bar{V}^{**} = -il\bar{P}^{**}(k, l) + \partial^2 \bar{V}^{**}/\partial Z^2 \tag{3.3c}$$

and the boundary conditions (2.6) become

$$\bar{U}^{**} = -\lambda F^{**}(k, l), \quad \bar{V}^{**} = \bar{W}^{**} = 0 \quad \text{at} \quad Z = 0, \tag{3.4a}$$

$$\bar{U}^{**} \to \lambda \bar{A}^{**}(k, l), \quad \bar{V}^{**} \sim \bar{D}^{**}(k, l)/\lambda Z \quad \text{as} \quad Z \to \infty, \tag{3.4b}$$

$$\bar{U}^{**}, \bar{V}^{**}, \bar{W}^{**}, \bar{P}^{**} \to 0 \quad \text{as} \quad X \to -\infty. \tag{3.4c}$$

The pressure–displacement relation is now

$$(k^2 + l^2)^{\frac{1}{2}} \bar{P}^{**} = k^2 \bar{A}^{**}. \tag{3.5}$$

As in Smith (1976*a*, *b*), the solution for $\bar{V}^{**}$ comes out first, from (3.3*c*), and is

$$\bar{V}^{**} = il\bar{P}^{**}(ik\lambda)^{-\frac{2}{3}} \mathscr{L}(t), \tag{3.6}$$

where

$$\mathscr{L}(t) = -\frac{2}{\sqrt{3}} \int_0^{\infty} \sin\left(\tfrac{1}{3}\xi^3 + \xi t - \tfrac{1}{6}\pi\right) d\xi, \quad t = (ik\lambda)^{\frac{1}{3}} Z \tag{3.7}$$

and $|\arg (ik\lambda)^n| < n\pi$. Then (3.3*a*, *b*) give

$$\frac{\partial \bar{U}^{**}}{\partial t} = \frac{l^2 \lambda \bar{P}^{**}}{(ik\lambda)^{\frac{5}{3}}} \mathscr{L}'(t) + B(k, l)\, \mathrm{Ai}\,(t), \tag{3.8}$$

where Ai is the Airy function and the unknown function $B(k, l)$ satisfies

$$B(k, l)\, \mathrm{Ai}'\,(0) + \lambda l^2 \bar{P}^{**}/(ik\lambda)^{\frac{5}{3}} = ik\bar{P}^{**}/(ik\lambda)^{\frac{2}{3}} \tag{3.9}$$

from (3.3*b*) at $Z = 0$. Integration of (3.8) with respect to Z from 0 to ∞, with (3.4), then yields

$$-\lambda F^{**} + \tfrac{1}{3} B(k, l) = \lambda \bar{A}^{**}. \tag{3.10}$$

Hence, from (3.9), (3.10) and (3.5) the pressure transform, in particular, is determined as

$$\bar{P}^{**}(k, l) = F^{**}(k, l)/[-(k^2 + l^2)^{\frac{1}{2}} k^{-2} + \gamma^{-\frac{4}{3}}(k^2 + l^2)\,(ik\lambda)^{-\frac{5}{3}}], \tag{3.11}$$

where $\gamma = (-3\mathrm{Ai}'(0))^{\frac{1}{3}} = 0{\cdot}8272$.

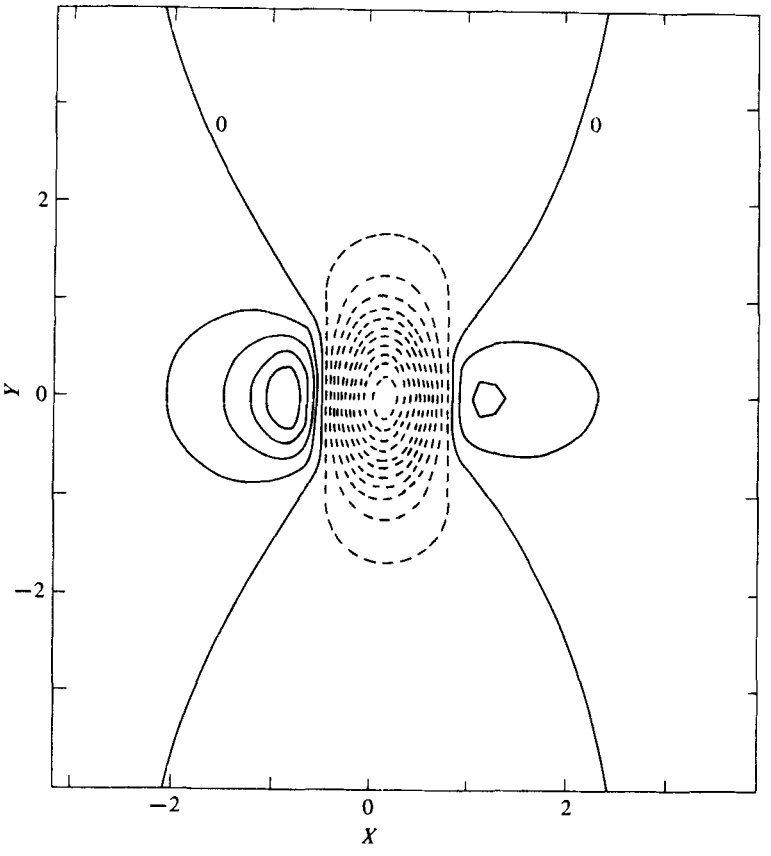

FIGURE 2. Curves of constant pressure $\bar{P}$. – – –, negative values; ——, positive values. The contour intervals are 0·02.

Given $\bar{P}^{**}$, $\bar{A}^{**}$ follows from (3.5), $\bar{D}^{**}$ from (2.2e) and the shear stresses at the surface, $\tau_X = \partial U(X, Y, O)/\partial Z$ and $\bar{\tau}_Y = \partial \bar{V}(X, Y, O)/\partial Z$, stem from (3.6) and (3.8). We omit the precise details. Also, the influence of the factor λ can be extracted by defining

$$(P, A, D, \tau_X, \bar{\tau}_Y) = (\lambda^{\frac{1}{2}} P_1, \lambda^{-\frac{3}{4}} A_1, \lambda^{\frac{1}{2}} D_1, \lambda \tau_{1X}, \lambda \bar{\tau}_{1Y})$$

so that the terms with subscript 1 are independent of λ. Below we omit the subscript 1 for convenience (or, equivalently, take $\lambda = 1$).

4. Linearized results and discussion

The results for a linearized hump are presented in figures 2–8. Rather than express the double inversion of (3.11) in a real closed form (as in Stewartson 1970; Smith 1973), it proved more flexible to use a fast-Fourier-transform (FFT) numerical approach available at the Meteorological Office, Bracknell. Various grid sizes and integration ranges were employed and their results compared, to ensure satisfactory accuracy. Also, two analytical checks supported the results obtained numerically. First, the two-dimensional case considered by Smith (1973, figure 3) was verified. Second, the results far from the hump compared favourably with the asymptotic solutions obtainable in closed analytic form [see (4.2)–(4.8) below].

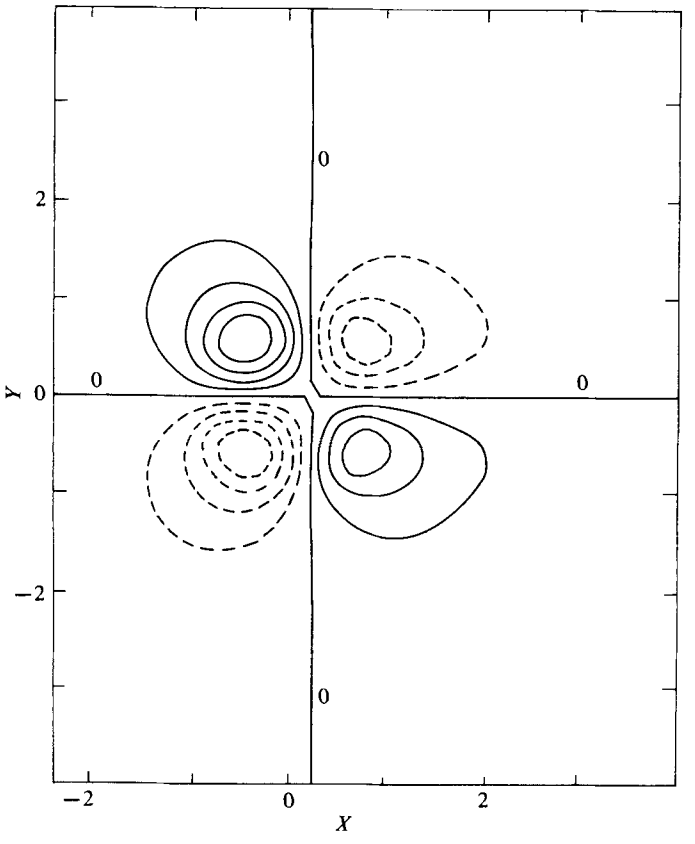

FIGURE 3. Curves of constant $\bar{D}$. Dashed and solid lines as in figure 2, with a contour interval of 0·02.

The three-dimensional shape studied was defined by

$$F(X, Y) = \begin{cases} \cos^2[\tfrac{1}{2}\pi(X^2+Y^2)^{\frac{1}{2}}] & \text{for} \quad X^2+Y^2 < 1, \\ 0 \quad \text{otherwise.} \end{cases} \tag{4.1}$$

Curves of constant pressure $\bar{P}$ are drawn in figure 2. Along the 'peak line' ($Y = 0$) the pressure exhibits the two-dimensional trend (Smith 1973), rising upstream, dropping fast over the front of the hump, reaching a negative minimum just behind the highest point and then rising fast on the leeward side before dropping slowly back to zero downstream. To the sides of the peak line the same trend emerges, but is less accentuated. Hence ahead of the hump, for example, a favourable pressure gradient is established in the $+Y$ direction (see next paragraph) for $Y > 0$. Far away, the flow acquires an essentially inviscid character as far as the pressures $\bar{P}$ and $\bar{D}$ are concerned and the hump acts as a delta function. Thus we find that, for $X^2+Y^2 \gg 1$,

$$\bar{P}(X, Y) \sim F^{**}(0, 0)\,(2X^2-Y^2)/2\pi(X^2+Y^2)^{\frac{5}{2}}, \tag{4.2a}$$

$$\bar{D}(X, Y) \sim -3F^{**}(0, 0)\,XY/2\pi(X^2+Y^2)^{\frac{5}{2}}. \tag{4.2b}$$

Constant-$\bar{D}$ curves are presented in figure 3. They give effectively the Y velocity v at the edge of the lower deck III, from (2.6*b*). Owing to the induced pressure gradient

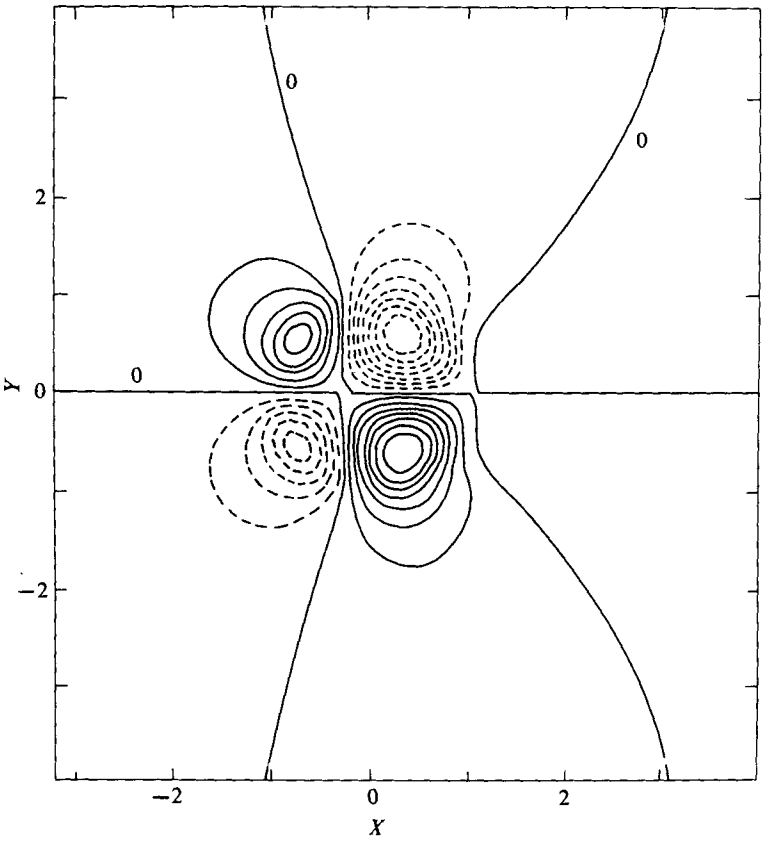

FIGURE 4. Constant-$\bar{\tau}_Y$ curves. Dashed and solid lines as in figure 2, with a contour interval of 0·02.

in the Y direction this Y slip is positive upstream. It changes sign near the peak of the hump, however, and thereafter is negative. Thus, at the edge of the lower deck, fluid is driven away from the peak line upstream, to enable the fluid to negotiate the obstacle, while downstream the slip effect is roughly the opposite. Simultaneously the whole secondary flow upstream in III moves outwards from the peak line, as the curves of azimuthal shear stress $\bar{\tau}_Y$ in figure 4 show. So the hump has a source-like effect on the secondary flow upstream (see below). Once the hump is encountered, $\bar{\tau}_Y$ reverses sign, reaching a negative minimum just beyond the hump's peak, and then becomes positive again immediately downstream of the hump. Hence, near the surface, fluid is drawn towards the area just leeward of the obstacle, before drifting outwards at a slower rate further downstream.

Figure 5 indicates the behaviour of the boundary-layer displacement $(-A(X, Y))$. Along and near the peak line the lower deck is displaced vertically upwards throughout the motion, with the maximum displacement occurring just after the hump's peak. Indeed, downstream the upward displacement appears to be confined broadly to a 'corridor' whose width in the Y direction is approximately that of the hump. Only close to the hump does the upward displacement exhibit any significant spreading from this corridor. The upward displacement there falls off quite rapidly in the Y direction, while upstream and downstream the displacement is downward outside the corridor.

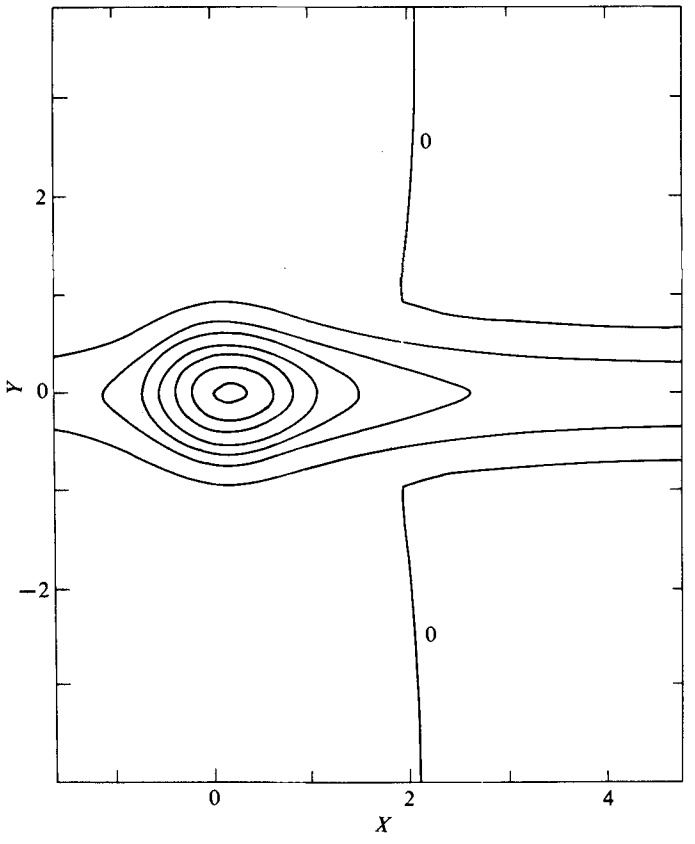

FIGURE 5. Constant-$\bar{A}$ curves. Dashed and solid lines as in figure 2, with a contour interval of 0·04.

The relatively small upward displacement near the peak line ahead of the hump is due to the pressure rise and the associated fall in axial shear stress (see below) there, whereas the downward motion away from the peak line seems to be necessary for mass conservation. Similar phenomena arise downstream, inside and outside the corridor, as the flow returns to its original two-dimensional state. Near the hump the increased displacement effects seem to be physically sensible because of the presence of the physical obstruction.

A corridor effect downstream is also evident in the axial shear stress τ_X (figure 6). Near the peak line τ_X drops slowly upstream, before rising rapidly over the front of the hump and falling even more rapidly at the rear. Downstream τ_X returns to its original value, from below in the centre of the corridor but from above near the edge of the corridor. The upstream trend here is in line with the pressure rise, and the ensuing development of τ_X is similar to that in a planar flow (Smith 1973). Outside the corridor downstream there are some curious effects. The most marked are the small zones far downstream where the axial shear stress rises slightly above the original value, in contrast with the stress deficit in the middle of the corridor. The cause seems to lie in the concentration of displacement in the corridor, whereas the axial and azimuthal pressure distributions are more widespread. The falling displacement dominates the behaviour in the corridor far downstream but has very little influence outside, where

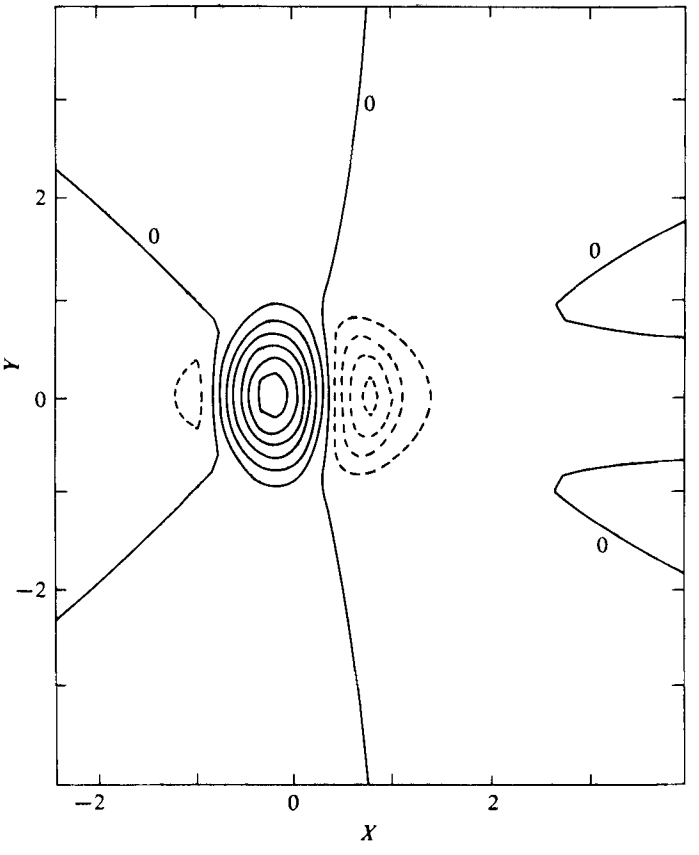

FIGURE 6. Curves of constant $(\tau_X - 1)/h$. Dashed and solid lines as in figure 2, with a contour interval of 0·1.

the two favourable horizontal pressure gradients combine to produce the overshoot in axial shear stress.

The existence of this corridor effect may be verified by analysing the flow properties far from the hump. When X (or Y) is large, the pressures $\bar{P}$ and $\bar{D}$ take on the virtually inviscid forms given in (4.2), since the boundary-layer displacement acquires a point-disturbance character ($\bar{A}^{**} \approx -F^{**}(0,0)$), so that the two pressures exhibit very little concentration or wake behaviour. By contrast, the residual displacement $\bar{A}$ and axial shear stress τ_X downstream for $X \gg 1$ are due totally to viscous action and do become concentrated in a wake or corridor, as follows. For the axial shear stress, given by

$$\frac{(\tau_X - 1)^{**}}{h} = \frac{3\,\mathrm{Ai}\,(0)\,(ik)^{\frac{2}{3}} F^{**}(k,l)}{(k^2+l^2)^{\frac{1}{2}}\,[1+\gamma^{-\frac{4}{3}}(ik)^{\frac{1}{3}}\,(k^2+l^2)^{\frac{1}{2}}]}\left\{\frac{k^2+l^2}{\gamma^{\frac{4}{3}}} - \frac{l^2}{9\,\mathrm{Ai}^2\,(0)}\right\}, \tag{4.3}$$

and for the displacement $\bar{A}$, the solution has quite distinct features when $X^2 + Y^2 \gg 1$ depending on whether or not Y is $O(1)$ with $X > 0$ (the region containing the corridor). When Y is large and $O(X)$, implying that $1 \gg l = O(k)$,

$$\frac{(\tau_X - 1)^{**}}{h} \approx 3\,\mathrm{Ai}\,(0)\,F^{**}(0,0)\frac{(ik)^{\frac{2}{3}}}{(k^2+l^2)^{\frac{1}{2}}}\left\{\frac{k^2}{\gamma^{\frac{4}{3}}} + \left(\gamma^{-\frac{4}{3}} - \frac{1}{9\,\mathrm{Ai}^2\,(0)}\right) l^2\right\}. \tag{4.4}$$

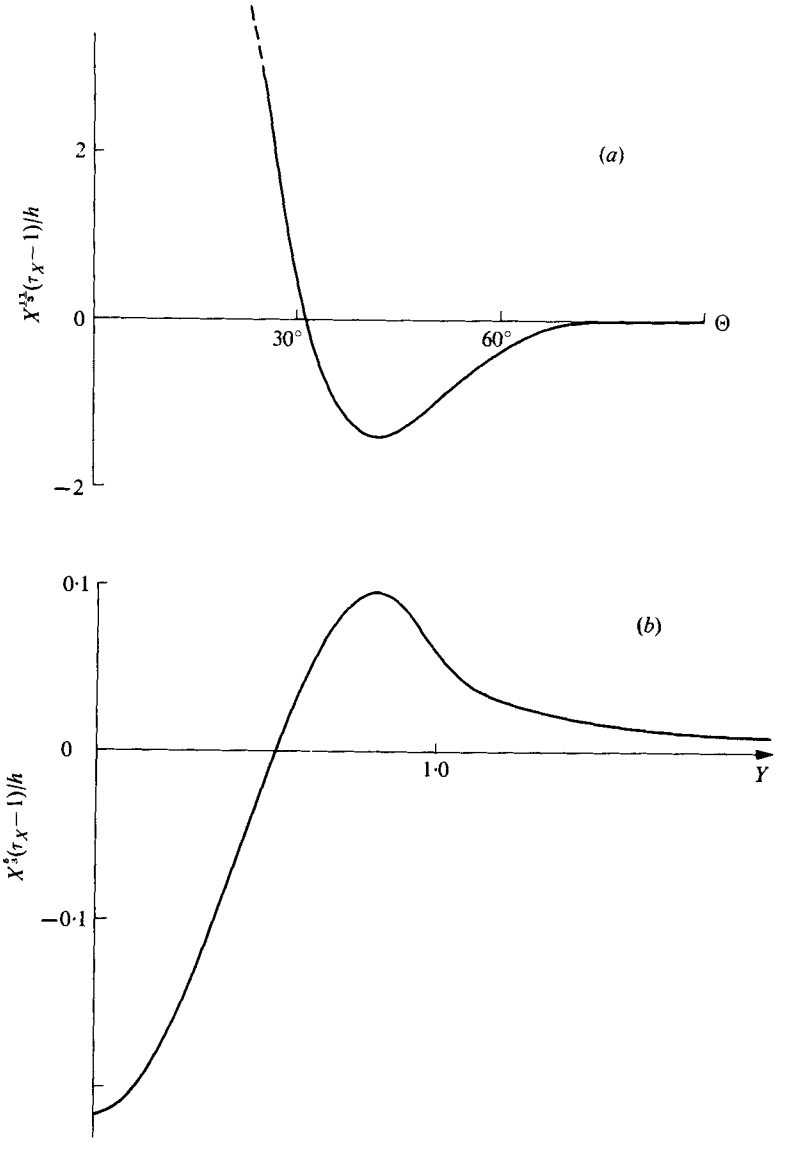

FIGURE 7. The axial skin friction far from the obstacle (*a*) when Θ is of order unity, outside the corridor, and (*b*) when Y is of order unity, inside the corridor.

The inverse transform of $(ik)^{\frac{2}{3}}(k^2+l^2)^{-\frac{1}{2}}$ is

$$\frac{2^{-\frac{1}{3}}}{\pi^2 Y^{\frac{5}{3}}}\left\{(\Gamma(\tfrac{5}{6}))^2\mathscr{F}\left(\tfrac{5}{6},\tfrac{5}{6};\tfrac{1}{2};-\frac{X^2}{Y^2}\right)-\frac{2\times 3^{\frac{1}{2}}X}{Y}(\Gamma(\tfrac{4}{3}))^2\mathscr{F}\left(\tfrac{4}{3},\tfrac{4}{3};\tfrac{3}{2};-\frac{X^2}{Y^2}\right)\right\}, \tag{4.5}$$

where $\mathscr{F}(a,b;c;\hat{z})$ is the hypergeometric function (Gradshteyn & Ryzhik 1965, p. 1039). If we denote (4.5) by $G(\hat{t})\,Y^{-\frac{5}{3}}$, where $\hat{t}=X^2/Y^2$, then

$$(\tau_X-1)/3\,\mathrm{Ai}\,(0)\,F^{**}(0,0)\,h \approx -\left\{\gamma^{-\frac{4}{3}}\frac{\partial^2}{\partial X^2}+\left(\gamma^{-\frac{4}{3}}-\frac{1}{9\,\mathrm{Ai}^2(0)}\right)\frac{\partial^2}{\partial Y^2}\right\}\frac{G(\hat{t})}{Y^{\frac{5}{3}}}$$
$$= X^{-\frac{11}{3}}H(\hat{t}), \quad \text{say.} \tag{4.6}$$

Hence $\tau_X - 1 \approx$ [function of $\Theta = \tan^{-1}(Y/X)$]$/X^{\frac{11}{3}}$. The function $H(\hat{t})$, drawn in figure 7(*a*), was calculated by evaluating $G(\hat{t})$ from the series expansions of the hypergeometric functions $\mathscr{F}$ and then differentiating numerically. However, at $\Theta = 0$ the function is singular and $H \sim \Theta^{-2}$ as $\Theta \to 0$. Hence a different representation is called for near the X axis, in fact when Y is $O(1)$. The dominant contribution to τ_X then comes from small values of k, with l finite, when

$$\frac{(\tau_X - 1)^{**}}{h} \approx 3\,\mathrm{Ai}\,(0)\left(\gamma^{-\frac{4}{3}} - \frac{1}{9\,\mathrm{Ai}^2\,(0)}\right)(ik)^{\frac{2}{3}}\,|l|\,F^{**}(0, l). \tag{4.7}$$

This gives

$$\frac{\tau_X - 1}{h} \approx -\frac{3^{\frac{2}{3}}\,\mathrm{Ai}\,(0)}{4\pi^2}\left(\gamma^{-\frac{4}{3}} - \frac{1}{9\,\mathrm{Ai}^2\,(0)}\right)\Gamma(\tfrac{5}{3})\,X^{-\frac{6}{3}}\int_{-\infty}^{\infty}\frac{g'(\eta)\,d\eta}{Y - \eta}, \tag{4.8}$$

where

$$g(Y) = \int_{-\infty}^{\infty} F(X, Y)\,dX$$

and the integrals have principal values. As $Y \to \infty$ now, $\tau_X - 1$ falls off like Y^{-2} and the solution (4.8) matches exactly with that in (4.6) as $\Theta \to 0+$. Numerical integration of (4.8) for the hump in (4.1) gives the graph in figure 7(*b*). The wake effect suggested by the previous global results is confirmed, since there is a corridor of approximately half the width of the hump in which the surface flow is retarded ($\tau_X < 1$). Outside this, and as far as 30° from the X axis, the surface flow is accelerated ($\tau_X > 1$). At greater values of Θ the surface flow is again decelerated, apart from in a small zone between approximately 80° and 130°, where there is a minor acceleration of the surface fluid. The corridor effect evident in the displacement $\bar{A}$ may be confirmed by a similar analysis, as can a corridor phenomenon occurring in $\bar{\tau}_Y$. The perturbation velocity $\bar{U}$ in the wake has the same Y profile as (4.8) and depends on the similarity variable $Z/X^{\frac{1}{3}}$. Its maximum decays as $X^{-\frac{4}{3}}$, as does $\bar{A}$, while $\bar{\tau}_Y \propto X^{-\frac{8}{3}}$ in the corridor. Outside the corridor, $\bar{\tau}_Y \propto (X^2 + Y^2)^{-\frac{11}{6}}$. No corridor occurs upstream, although the original results did show some concentration there (because of the FFT's periodic nature in the axial direction) which has to be neglected.

Aside from the very existence of the corridor effect, several other points stand out. First, the velocity deficit in the corridor decays more slowly ($\propto X^{-\frac{7}{3}}$) than in the wake behind a two-dimensional hump (where the decay is like $X^{-\frac{7}{3}}$; Smith 1973). Second, the pressure gradient is insignificant in the corridor, decaying faster than the inertial forces, whereas in the planar case the pressure gradient itself determines the rapid decay. Third, the corridor does not spread significantly downstream [being confined to $|Y| \leqslant 0{\cdot}53$ for the hump (4.1)]. Intuitively one would expect any viscous effect, such as the corridor, to spread out as the distance downstream increases, owing to lateral convection and viscous diffusion. Here, however, the lateral convection is small because h is small, the viscous diffusion laterally is small owing to the shallowness of the hump (cf. Jackson's (1973) analysis of a narrow wake in a boundary layer with lateral diffusion as important as vertical diffusion) and both are overwhelmed by the concentrated displacement of the boundary layer behind the hump, producing a corridor of constant width. Fourth, the precise details of the corridor flow, even far downstream, do depend on those of the hump itself [from (4.8)], whereas most of the flow outside the corridor is of a global, inviscid kind and therefore is dependent only on the hump's total volume, i.e. the constant $F^{**}(0, 0)$ in (4.6).

The secondary flow (v, w) diagrams in figure 8 confirm many of the above aspects.

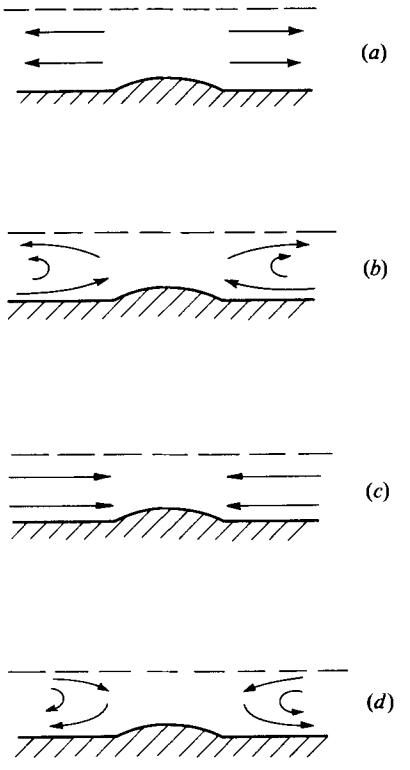

FIGURE 8. Secondary-flow sketches for the hump (4.1). Secondary velocities (v, w) are shown (*a*) upstream of the hump, (*b*) on its forward face, (*c*) on the hump's leeward side and (*d*) behind the hump. The dashed line indicates the upper edge of the lower deck.

The simple source-like trend upstream is followed by some major adjustments near the hump. First, fluid near the surface starts to be drawn inwards (towards the peak line) near the hump's peak, so that a vortex motion appears. Then, over the back of the hump, the entire lower-deck flow acquires a sink-like form, in order that the fluid may encircle the obstacle. Finally, beyond the hump, the displacement forces the surface fluid eventually to be expelled, while the fluid above the lower deck is drawn in, and so another vortex motion is set up. This vortex rotates in the opposite sense to the flatter, faster-decaying vortex near the rear of the hump (cf. Smith 1976*a*, *b*) and is generated by the vorticity interaction between the shear perturbation and the basic shear (as in the horseshoe vortices of Sedney 1973).

Further details of the linearized theory will be given by Brighton (1977) and Sykes (1978). We believe that a number of further investigations are suggested by this work. Other shapes need to be considered, to investigate the influence of symmetry with respect to the X axis in (4.1). More significant developments however are those concerned with the nonlinear problem of §2, where separation seems likely, or with stratification effects or three-dimensional oncoming profiles, all of which are more applicable to atmospheric dynamics and aerodynamics, for example.

Professor O. R. Burggraf has informed us of his investigations of the supersonic

analogue of the three-dimensional triple deck. One of us (P.W.M.B.) is grateful to the Science Research Council for financial support.

REFERENCES

BRIGHTON, P. W. M. 1977 Ph.D. thesis, University of Cambridge (to be submitted).

GRADSHTEYN, I. S. & RYZHIK, I. M. 1965 *Tables of Integrals, Series and Products.* Academic Press.

JACKSON, P. S. 1973 The flow round obstacles in boundary layers. Ph.D. thesis, University of Cambridge.

SEDNEY, R. 1973 A survey of the effects of small protuberances on boundary layer flows, *A.I.A.A. J.* **11**, 782.

SMITH, F. T. 1973 Laminar flow over a small hump on a flat plate. *J. Fluid Mech.* **57**, 803.

SMITH, F. T. 1976*a* Pipeflows distorted by nonsymmetric indentation or branching. *Mathematika* **23**, 62.

SMITH, F. T. 1976*b* On entry-flow effects in bifurcating, blocked or constricted tubes. *J. Fluid Mech.* **78**, 709.

SMITH, F. T. & STEWARTSON, K. 1973 On slot-injection into a supersonic laminar boundary layer. *Proc. Roy. Soc.* A **332**, 1.

STEWARTSON, K. 1970 On laminar boundary layers near corners. *Quart. J. Mech. Appl. Math.* **23**, 137.

STEWARTSON, K. 1974 Multi-structured boundary layers on flat plates and related bodies. *Adv. in Appl. Mech.* **14**, 145.

STEWARTSON, K. & WILLIAMS, P. G. 1969 Self-induced separation. *Proc. Roy. Soc.* A **312**, 181.

SYKES, R. I. 1978 Ph.D. thesis, University of London (to be submitted).